Available online at www.sciencedirect.com
SCIENCE DIRECT®
PERGAMON
International Journal of Impact Engineering 30 (2004) 193–204
INTERNATIONAL JOURNAL OF IMPACT ENGINEERING
www.elsevier.com/locate/ijimpeng

A modified model for the penetration into moderately thick plates by a rigid, sharp-nosed projectile

Q.M. Li[a,*], H.J. Weng[b], X.W. Chen[b]

[a] *Department of Mechanical, Aerospace and Manufacturing Engineering, UMIST, Room P/C25, Pariser Building, PO Box 88, Manchester M60 1QD, UK*

[b] *School of Civil and Environmental Engineering, Nanyang Technological University, Nanyang Avenue, Singapore 639798, Singapore*

Received 18 April 2002; received in revised form 18 October 2002; accepted 12 May 2003

Abstract

The deep penetration model based on cavity expansion analysis (Int. J. Impact Eng. 27 (2002) 619) is modified to take account of the increase of the contact area between the projectile nose and the target medium before the projectile nose fully penetrates into the target. The modified penetration model is applicable to those penetration problems where the length of the projectile nose is comparable to the penetration depth. The predicted results are in good agreement with experimental results from Diskshit and Sundararajan (Int. J. Impact Eng. 12(3) (1992) 373) and Diskshit et al. (Int. J. Impact Eng. 16(2) (1995) 293).

Keywords: Penetration; Analytical model; Rigid projectile

1. Introduction

Dynamic cavity expansion model has been applied to formulate the target resistance in deep penetration problems of various target materials (e.g., [1–5]). Recently, Chen and Li [6] and Li and Chen [7] presented dimensionless formulae to predict the penetration depth into various target materials by a rigid projectile of a wide range of nose shapes, in which two dimensionless numbers were introduced based on dynamic cavity expansion theory. In the formulation of Chen and Li [6], the continuous increase of the contact area between the projectile nose and the target medium, as shown in Fig. 1, is neglected before the projectile nose enters the target material

*Corresponding author. Fax: +44-161-200-3849.
E-mail address: qingming.li@umist.ac.uk (Q.M. Li).

0734-743X/03/$ - see front matter
doi:10.1016/S0734-743X(03)00067-8

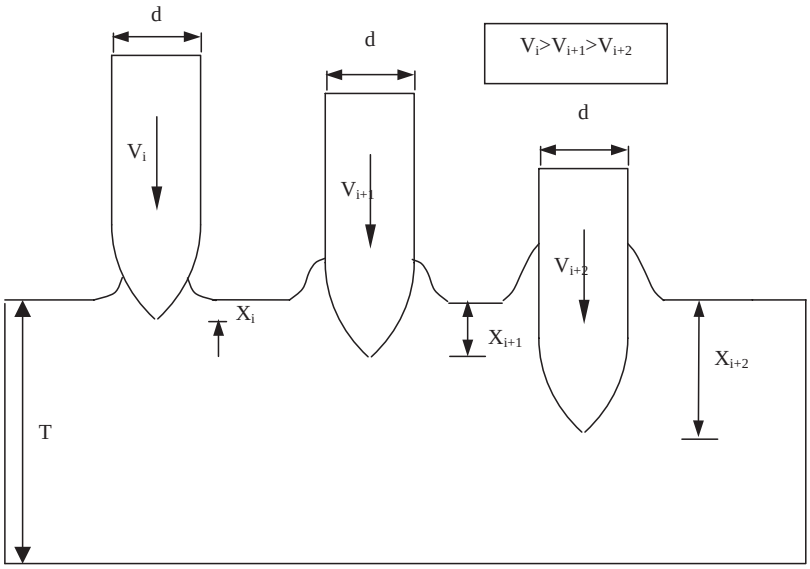

Fig. 1. Penetration process of an ogive-nose projectile into the plate.

completely. Thus, the proposed formulae are only applicable to deep penetration. When the penetration depth is comparable with the projectile nose length in a penetration problem or in the penetration stage of a multi-stage perforation process, the increased contacting area between the projectile nose and target material may need to be considered.

Dikshit and Sundararajan [8] conducted a series of laboratory tests for the penetration of thick steel plates by ogive-shaped projectiles, where the plate thickness is in the same order of the nose length of the projectile. In this case, the change of the contact area between the projectile nose and the target material during the entrance process must be considered in the formulation of the penetration resistance. Dikshit and Sundararajan [8] used an energy-based model to predict experimental results, which was further modified by Liaghat and Malekzadeh [9] for the calculation of a plastic zone in target medium in front of the projectile nose. Although, the prediction based on Dikshit and Sundararajan's [8] model gives a good agreement with experimental results, it requires more material parameters together with an empirical equation to determine the size of the plastic zone, which is not in favor of engineering applications.

In the present paper, the penetration resistance in [6] is modified to take into account the continuous increase of the contact area between the projectile nose and the target medium during the stage before the projectile nose enters the target completely. The modified model is used to predict the penetration depth of an ogive-shaped rigid projectile into steel plates of varying thicknesses and hardnesses conducted by Dikshit and Sundararajan [8] and Dikshit et al. [10], in which the projectile nose length is in the same order of the penetration depth, and thus, the embedment of the projectile nose into the target is comparable with the nose length of the projectile. Good agreements are found between the predicted results of the analytical model and the experimental results.

2. The modified penetration model

Based on the dynamic cavity expansion theory, the penetration resistance of the target medium on the projectile nose can be expressed by [11,6]

$$F_x = \frac{\pi d^2}{4}(A\sigma_y N_1 + B\rho V^2 N_2), \tag{1}$$

where σ_y and ρ are the yielding stress and density of the target material, respectively, d is the shank diameter of the projectile, A and B are dimensionless constants as described in the later part of this section, and V is the instant velocity of projectile in penetration process. The orientation of the coordinates (x, y) is defined in Fig. 2. N_1, N_2 and N^* are dimensionless parameters depending on the nose shape of the projectile [6]:

$$N_1 = 1 + \frac{8\mu_m}{d^2}\int_0^h y\,\mathrm{d}x, \tag{2a}$$

$$N_2 = N^* + \frac{8\mu_m}{d^2}\int_0^h \frac{yy'^2}{1+y'^2}\,\mathrm{d}x, \tag{2b}$$

$$N^* = -\frac{8}{d^2}\int_0^h \frac{yy'^3}{1+y'^2}\,\mathrm{d}x, \tag{2c}$$

where h is the height of nose, as shown in Fig. 2, μ_m is the friction coefficient. If friction is ignored, $N_1 = 1$, $N_2 = N^*$. Various formulae of N_1, N_2 and N^* for different nose shapes, e.g., cone, ogive, hemispherical-nose, and truncated-ogive, can be found in [6]. Eqs. (1) and (2) require the satisfaction of the following assumptions:

(a) Projectile is rigid, i.e., they will not deform during penetration process.
(b) Projectile strikes the target normally.
(c) No friction exists along the projectile shank.
(d) The rear free surface has negligible influence on the penetration resistance throughout the penetration process.

Furthermore, the validity of Eqs. (1) and (2) also requires that the projectile nose is completely penetrated into the target medium. When the total penetration depth is in the same order of the

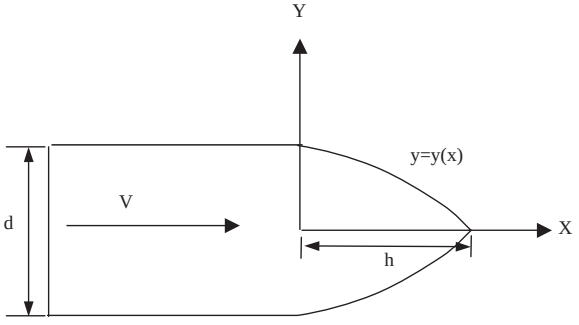

Fig. 2. Profile of the ogive-nose projectile.

height of the projectile nose, the contact area depends on the penetration depth, and thus, the penetration resistance also depends on the penetration depth.

The modified penetration resistance with considering the change of the contact area between the projectile nose and the target medium before the projectile nose enters the target completely is

$$F(x) = \pi y^2 (A\bar{N}_1\sigma_y + B\bar{N}_2\rho V^2) \tag{3}$$

when $d/2$ is replaced by y in Eqs. (1) and (2), where

$$\bar{N}_1 = 1 + \frac{2\mu_m}{y^2}\int_x^h y\,\mathrm{d}x, \tag{4a}$$

$$\bar{N}_2 = \bar{N}^* + \frac{2\mu_m}{y^2}\int_x^h \frac{yy'^2}{1+y'^2}\,\mathrm{d}x, \tag{4b}$$

$$\bar{N}^* = -\frac{2}{y^2}\int_x^h \frac{yy'^3}{1+y'^2}\,\mathrm{d}x. \tag{4c}$$

Specially, when the nose of the projectile has a profile equation $y = a \times (h-x)^{1/2} + b$, where $h = 0.02\,\mathrm{m}$ is the length of the nose, $a = 0.0707\,\mathrm{m}^{1/2}$, $b = 0$, according to Fig. 1 of [8], the geometric factors can be expressed as

(a) For penetration depth $(x_\mathrm{p}) < h$, where $x_\mathrm{p} = h - x$:

$$N_1 = 1 + \frac{4\mu_m a}{3y^2}(h-x)^{1.5}, \tag{5a}$$

$$\bar{N}_2 = \bar{N}^* + \frac{\mu_m a^3}{2y^2}\left[2\sqrt{h-x} - a^* \arctan\left(\frac{2}{a}\sqrt{h-x}\right)\right], \tag{5b}$$

$$\bar{N}^* = \frac{a^4}{4y^2}\left[\ln\left(h - x + \frac{a^2}{4}\right) - \ln\left(\frac{a^2}{4}\right)\right]. \tag{5c}$$

(b) For penetration depth $(x_\mathrm{p}) \geqslant h$:

$$\bar{N}_1 = 1 + \frac{16\mu_m a}{3d^2}(h)^{1.5}, \tag{6a}$$

$$\bar{N}_2 = \bar{N}^* + \frac{2\mu_m a^3}{d^2}\left[2\sqrt{h} - a^* \arctan\left(\frac{2}{a}\sqrt{h}\right)\right], \tag{6b}$$

$$\bar{N}^* = \frac{a^4}{d^2}\left[\ln\left(h + \frac{a^2}{4}\right) - \ln\left(\frac{a^2}{4}\right)\right]. \tag{6c}$$

Parameters A and B in Eqs. (1) and (3) are the material constants of the target. Forrestal et al. [5] obtained spherically symmetric cavity-expansion results for a compressible elastic–perfectly plastic material. For both incompressible ($v = 1/2$) and compressible ($v \neq 1/2$) materials, parameter A is expressed as [1,6]

$$A = \frac{2}{3}\left\{1 + \ln\left[\frac{E}{3(1-v)\sigma_y}\right]\right\}. \tag{7}$$

Parameter B depends mostly on the compressibility of the target material and it ranges from 1.0 to 1.5; $B = 1.5$ for incompressible elastic–plastic material [1,6]).

For the coefficient of friction μ_m, two opinions exist. The first assumes that μ_m is a constant and its values may vary between 0 to 0.3. The second assumes that μ_m decreases with increasing sliding velocity between the projectile and the plate target [8]. Although the second opinion is more realistic than the first one, the actual relationship between the friction coefficient and the sliding velocity is so far uncertain, and therefore, a constant μ_m value is assumed in the present study.

The relationship between the increment of kinetic energy of projectile and the work done by the axial force acting on the projectile nose is defined as

$$\Delta E_k = -F_x(x)\Delta x. \tag{8}$$

The initial kinetic energy of the projectile is

$$E_k = \tfrac{1}{2} M V_0^2, \tag{9}$$

where M is the mass of the projectile and V_0 is the initial impacting velocity.

3. Numerical calculations

Penetration depth x_p can be determined by Eqs. (3), (8) and (9). However, due to the complexity of these equations, analytical solution for the penetration depth is not feasible. In this study, numerical method is used to solve the problem. It is assumed that the whole penetration process can be divided into a number of steps, each with a small constant penetration depth Δx. Under this assumption, the following set of equations can be obtained at any specified step i:

$$x_i = i\,\Delta x, \tag{10}$$

$$\Delta E_i = -F_x(x)\,\mathrm{d}x = -\Delta x\left[\frac{F(x_{i-1}) + F(x_i)}{2}\right], \tag{11}$$

$$\Delta E_i = \tfrac{1}{2} M(V_i^2 - V_{i-1}^2), \tag{12}$$

and

$$F(x_i) = \pi y_i^2 (A(\bar{N}_1)_i \sigma_y + B(\bar{N}_2)_i \rho V_i^2). \tag{13}$$

Hence the projectile velocity (V_i) at step i can be expressed using the following equation:

$$V_i = \sqrt{\frac{0.5MV_{i-1}^2 - 0.5\Delta x\left[\pi y_i^2 A(\bar{N}_1)_i \sigma_y + \pi y_{i-1}^2 A(\bar{N}_1)_{i-1}\sigma_y + \pi y_{i-1}^2 B(\bar{N}_2)_{i-1}\rho V_{i-1}^2\right]}{0.5\pi y_i^2 B(\bar{N}_2)_i \rho\,\Delta x + 0.5M}}. \tag{14}$$

Assuming that at step $i = k$, the velocity decreases to zero, the total penetration depth can be calculated as

$$x_p = k\,\Delta x. \tag{15}$$

The accuracy of the x_p depends on the value of Δx. In the present study, Δx is taken as 0.01 mm, which is small enough to obtain a precise penetration depth.

4. Comparisons with experimental data and discussion

The predicted penetration depths from present analytical model are compared with previously published penetration data for 20, 40 and 80 mm thick plates of different hardnesses by Dikshit and Sundararajan [8] and Dikshit et al. [10]. Rolled homogeneous armous (RHA) plates are used as the target, which has density $\rho = 7800\,\mathrm{kg/m^3}$, Young's modulus $E = 200\,\mathrm{GPa}$ and Poisson's ratio $v = 0.3$.

Dikshit and Sundararajan [8] tested 20, 40 and 80 mm thick plates with various Vickers hardnesses HV350 $\pm$ 10, HV315 $\pm$ 10 and HV295 $\pm$ 10, and correspondingly, the yield strengths are 1060, 920 and 860 MPa. Dimensionless parameter A for 20, 40 and 80 mm thick plates can be obtained by applying Eq. (7), i.e., 3.653, 3.760 and 3.805, respectively. The influence of parameter B on the model prediction was examined for different values B between 1.0 and 1.5 for a given value of μ_m between 0 and 0.2. It was found that the dimensionless parameter B has a minor effect on the penetration depth for the cases studied, as shown in Fig. 3.

Since it is difficult to investigate the effect of sliding friction experimentally and no reliable laboratory data are available for the kinetic value of μ_m, a parametric analysis is conducted to show the influence of μ_m on penetration. Fig. 3 shows the comparisons of predicted penetration depths for 80 mm plates when μ_m varies from 0 to 0.2, which covers the possible range of the kinetic friction coefficient in the studied problem, e.g., some values of μ_m between projectile and aluminum–alloy target were summarized in [6]. Although the predicted penetration depths have noticeable variation when μ_m varies in a broad range between 0 and 0.2, this variation is acceptable in a penetration problem, and therefore, best fitting value $\mu_m = 0.1$ and $B = 1.0$ were used in calculations.

For penetration of relatively thick plates, it is assumed that projectile is effectively resisted by plates, i.e., the plastic zone remains confined, throughout the penetration process. Once the plastic zone reaches the back face of the plate, i.e., bugle starts to occur, the resistance offered by the plate drops rather dramatically [8]. Thus, concept of effective thickness of plates (T_e) is

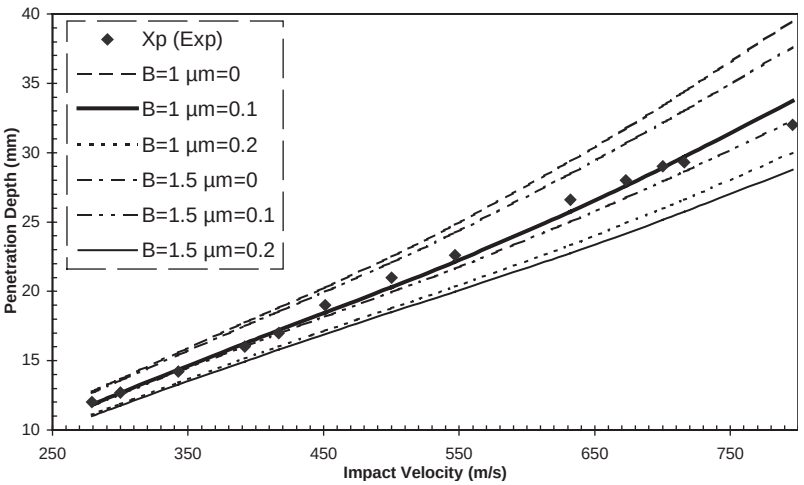

Fig. 3. Comparisons of predicted penetration depths for 80 mm plates with different values of B and μ_m [8].

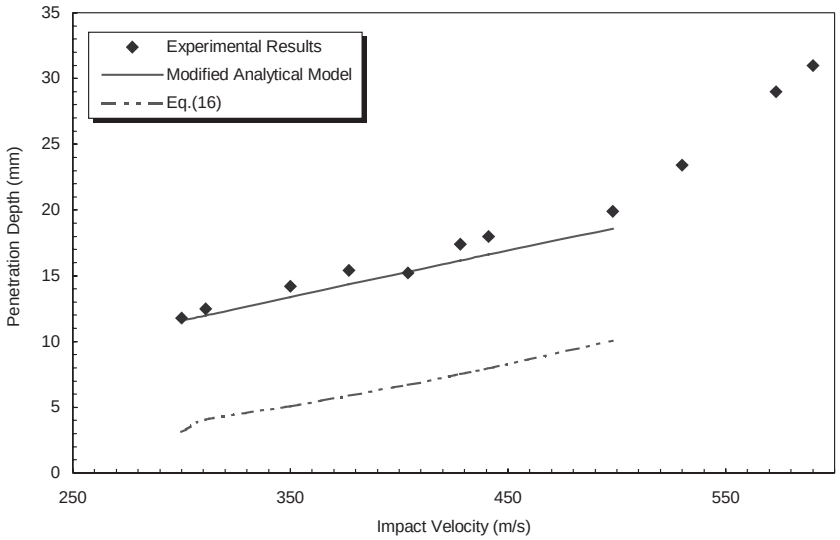

Fig. 4. The variation of the depth of penetration (X_p) with impact velocity in 20 mm plate of HV350 [8].

introduced, which refers to the maximum penetration depth before the plastic zone reaches the back face of the plate. The value of T_e is about 13, 26 and 60 mm for 20, 40 and 80 mm plates, respectively [8]. Most experimental penetration depths for 40 and 80 mm plates from [8] are less than the effective thickness of the plates; hence it can be treated as penetration of thick plates. However, some of the penetration depths of 20 mm thick plate are greater than its effective thickness, which may restrict the application of the present model, as shown in Fig. 4, when the impact velocity is greater than 500 m/s.

The analytical model works well for the prediction of the penetration depth of 40 and 80 mm thick plates because the final penetration depths are normally smaller than the effective thicknesses of the 40 and 80 mm thick plates. Figs. 5 and 6 show the comparisons between the predictions of the penetration depth from the present analytical model and the experimental penetration data by Dikshit and Sundararajan [8]. Good agreements between them are observed. Chen and Li's [6] formula of penetration depth for deep penetration

$$\frac{x}{d} = \frac{2}{\pi} N \ln\left(1 + \frac{I}{N}\right), \tag{16}$$

which ignores the entering stage of the projectile nose into the target, is also shown in Figs. 5 and 6, in which, $I = (1/AN_1)MV_0^2/d^3\sigma_y$, $N = (1/BN_2)M/\rho d^3$ and N_1, N_2 and N^* are given by Eqs. (2a)–(2c). It is shown that the present penetration model improves Chen and Li's [6] predictions considerably, which implies that the proposed modification is necessary for the studied penetration problem.

Fig. 4 shows that the experimental penetration depth becomes slightly larger than the predicted value when the penetration depth is greater than the effective thickness of the plate. However, the difference between the predictions and the measured penetration depths is small until the penetration depth approaches to the thickness of the plate.

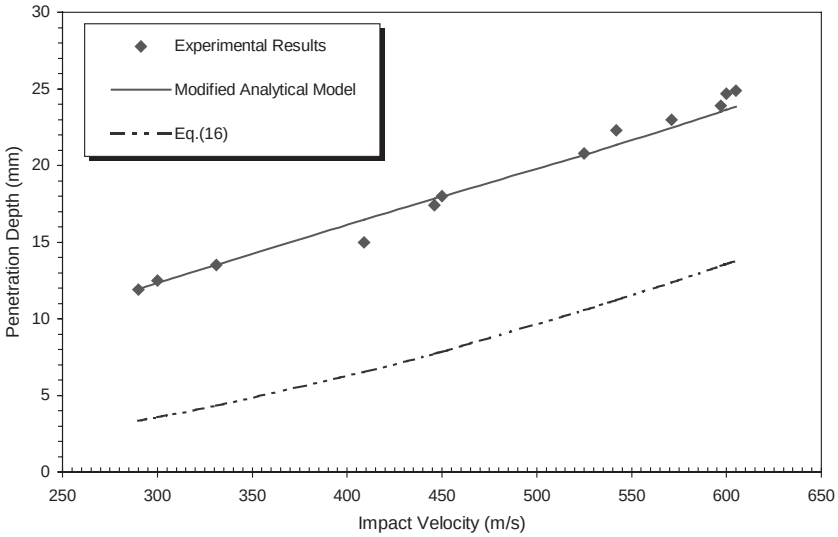

Fig. 5. The variation of the depth of penetration (X_p) with impact velocity in 40 mm plate of HV315 [8].

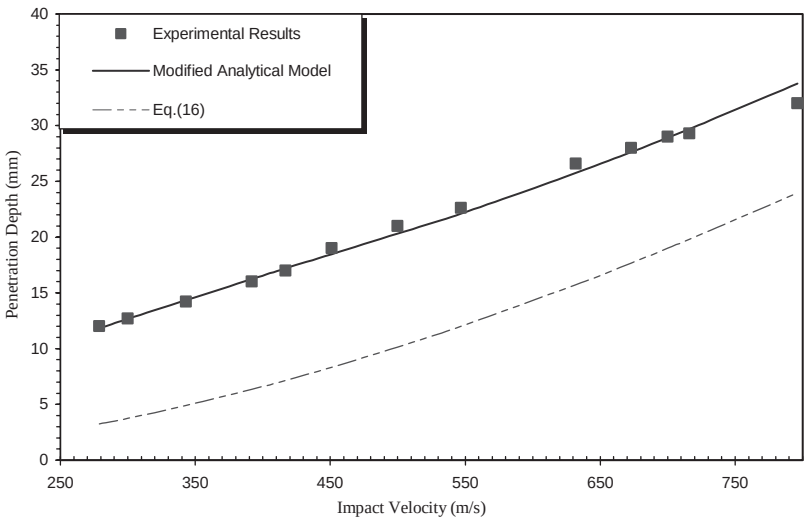

Fig. 6. The variation of the depth of penetration (X_p) with impact velocity in 80 mm plate of HV295 [8].

The histories of the force exerted on the projectile, the histories of the projectile velocity and penetration depth are shown in Figs. 7–9 for the penetration into 80 mm plates at $V_0 = 300$, 550 and 800 m/s. As shown in Fig. 7, for the cases of high impact velocities, i.e., $V_0 = 550$ m/s and 800 m/s, the resistant force first increases to their maximum value, and then converges slowly to a stationary value of $F_s = (\pi d^2/4)A\sigma_y$. In this case, the nose of the projectile immerses completely into the target at the end of the penetration event. On the contrary, for the case of small impact velocity, i.e., $V_0 = 300$ m/s, the resistant force keeps monotonously increasing until its maximum,

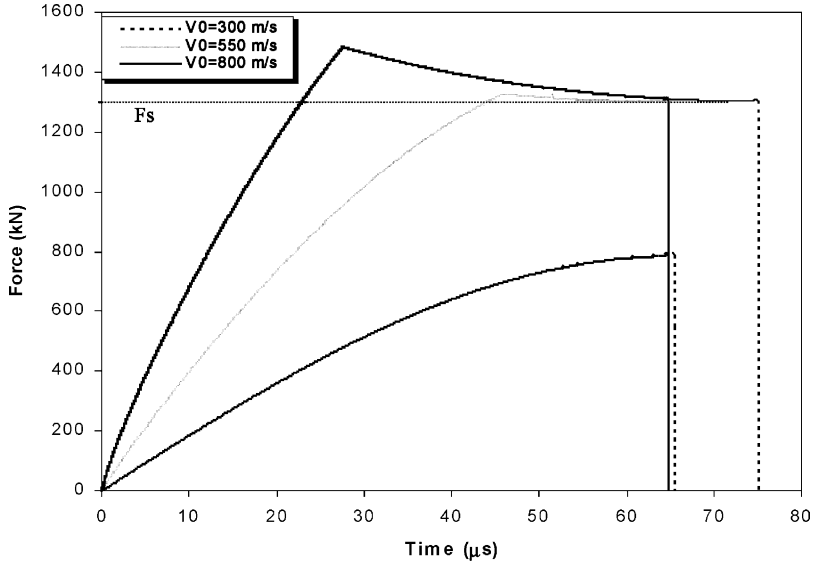

Fig. 7. The force–time history for penetration of 80 mm plates of HV295 at $V_0 = 300$, 550 and 800 m/s, where $F_s = \pi(0.5d)^2 AN_1\sigma_y$.

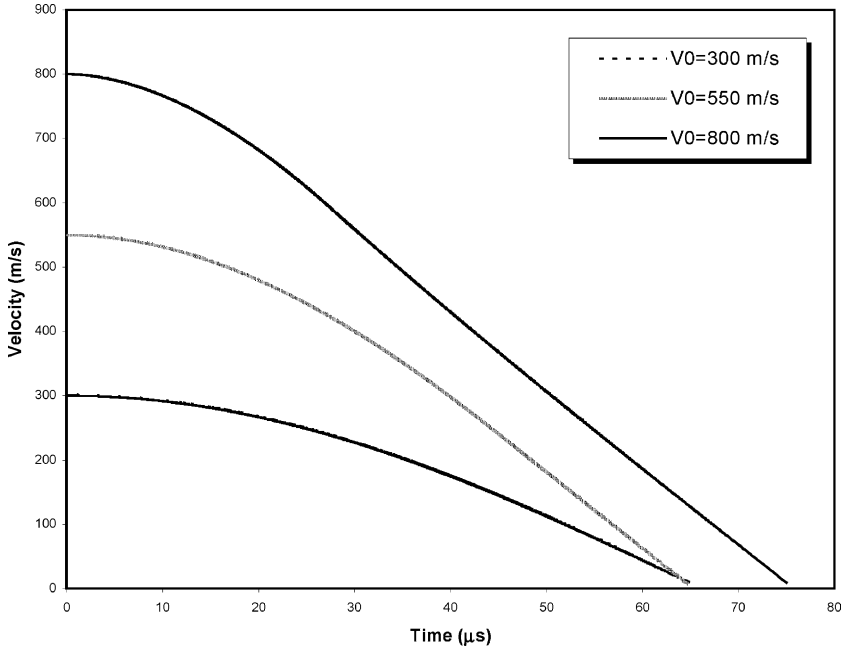

Fig. 8. The projectile velocity–time history for penetration of 80 mm plates of HV295 at $V_0 = 300$, 550 and 800 m/s.

where only part of the projectile nose immerses into the target at the end of penetration. The initial increasing of resistance is due to the increase of the contact area between the nose of the projectile and the target. After the nose of the projectile immerses completely into the target,

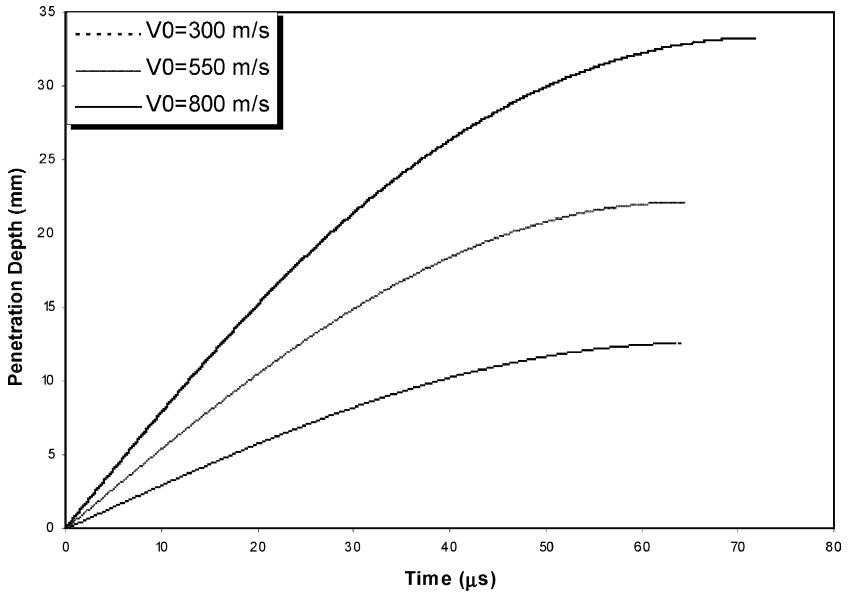

Fig. 9. The penetration depth–time history for penetration of 80 mm plates of HV295 at $V_0 = 300$, 550 and 800 m/s.

the first term on the right side of Eq. (3) remains constant and is equal to $F_s = (\pi d^2/4)A\sigma_y$. Thus, total resistant force decreases with velocity. All three curves drop to zero as soon as the projectiles terminate in the target.

Dikshit et al. [10] further tested 20 and 80 mm thick plates with various Vickers hardnesses using the same experimental setup. Figs. 10 and 11 give the variation of penetration depth with impact velocity in 20 and 80 mm steel plates, where the yield strengths of HV300/295, HV350, HV440 and HV520 steel plates are 800, 1080, 1500 and 1625 MPa, respectively, according to Fig. 1 in [10]. Other parameters are the same as their early specifications in [8].

All test data of 80 mm thick plates and part of test data of 20 mm thick plates are within the range of effective thickness of plates (T_e). However, some test data of 20 mm thick plates are beyond the effective thickness of plates (T_e), as shown in Fig. 10, when the impact velocity is greater than a velocity around 450–500 m/s, which confines the application of the present model.

For both 20 and 80 mm thick plates of hardnesses between HV300 and HV440, the analytical model gives good prediction for the penetration depth as long as the final penetration depth is not beyond the effective thickness of the specified plate. However, for both 20 and 80 mm thick steel plates of HV520, the analytical model overestimates the penetration depth. Obviously, ductile hole-enlargement is not the penetration mechanism in those cases. As denoted by Dikshit et al. [10], adiabatic shear band (ASB) failure and the substantial deformation of projectile may dominate the whole local impact process when the projectile strikes harder plates. This may be responsible for the mismatch between predictions and experimental results for the hardest plates in Figs. 10 and 11. However, other factors, such as strain rate, temperature and damage, may also contribute to these discrepancies, which require more advanced model to deal with.

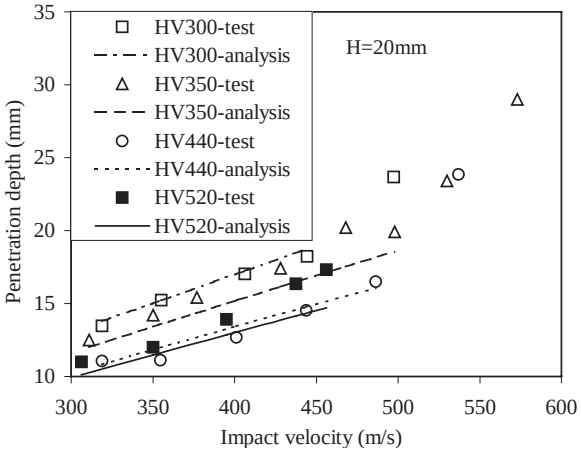

Fig. 10. The variation of penetration depth with impact velocity in 20 mm plate (referred to [10]).

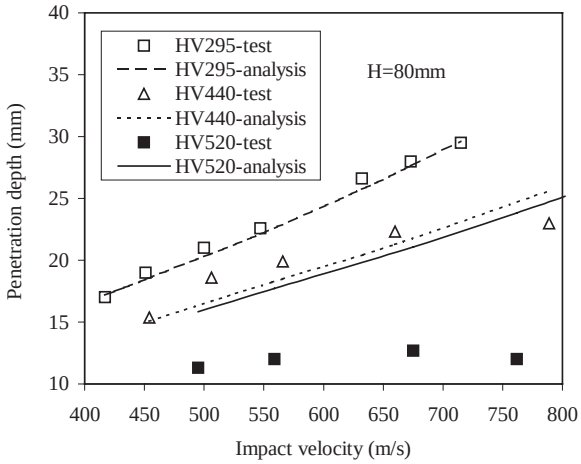

Fig. 11. The variation of penetration depth with impact velocity in 80 mm plate (referred to [10]).

General approaches with considering the immersing and leaving processes of the rigid projectile into target have been presented in other researches [12–16]. These general approaches have been applied to prove the area rule in order to find error to use a simple/regular nose shape to approach a complex nose shape [12,13] and to optimise projectile nose shapes in order to obtain maximum ballistic performances [15,16]. The present model is much simpler than those general approaches, but leads to good predictions when comparing with experimental results.

5. Conclusions

In this study, a modification is made on an analytical penetration model based on dynamic cavity expansion theory [6]. The analytical results are compared with the experimental results for

the penetration of rigid, ogive-shaped projectile against steel plates of various thicknesses over a velocity range between 300 and 800 m/s. Good agreements between the predictions of the present model and the experimental results from [8,10] are observed. Significant differences between the predictions of Chen and Li's [6] model and corresponding experimental results were observed, which implies that the modification of Chen and Li's [6] model is necessary when the penetration depth is comparable to the nose length of the projectile.

Acknowledgements

First author acknowledges beneficial discussion with Professor T. Elperin on penetration mechanics and appreciates his comments.

References

[1] Forrestal MJ, Luk VK. Dynamic spherical cavity-expansion in a compressible elastic–plastic solid. ASME J Appl Mech 1988;55:275–9.
[2] Forrestal MJ, Luk VK. Penetration into soil targets. Int J Impact Eng 1992;12:427–44.
[3] Luk VK, Forrestal MJ, Amos DE. Dynamics spherical cavity expansion of strain-hardening materials. ASME J Appl Mech 1991;58(1):1–6.
[4] Forrestal MJ, Altman BS, Cargile JD, Hanchak SJ. An empirical equation for penetration depth of ogive-nose projectiles into concrete targets. Int J Impact Eng 1994;15(4):395–405.
[5] Forrestal MJ, Tzou DY, Askari E, Longcope DB. Penetration into ductile metal targets with rigid spherical-nose rods. Int J Impact Eng 1995;16(5/6):699–710.
[6] Chen XW, Li QM. Deep penetration of a non-deformable projectile with different geometrical characteristics. Int J Impact Eng 2002;27:619–37.
[7] Li QM, Chen XW. Dimensionless formulae for penetration depth of concrete target impacted by a non-deformable projectile. Int J Impact Eng 2003;28(1):93–116.
[8] Diskshit SN, Sundararajan G. The penetration of thick steel plates by ogive shaped projectile—experiment and analysis. Int J Impact Eng 1992;12(3):373–408.
[9] Liaghat GH, Malekzadeh A. A modification to the mathematical model of perforation by Dikshit and Sundararajan. Int J Impact Eng 1999;22:543–50.
[10] Dikshit SN, Kutumbarao VV, Sundararajan G. The influence of plate hardness on the ballistic penetration of thick steel plates. Int J Impact Eng 1995;16(2):293–320.
[11] Jones SE, Rule WK. On the optimal nose geometry for a rigid penetrator, including the effects of pressure-dependent friction. Int J Impact Eng 2000;24:403–15.
[12] Ben-Dor G, Dubinsky A, Elperin T. Area rules for penetrating impactors. Theor Appl Fract Mech 1997;26:193–8.
[13] Ben-Dor G, Dubinsky A, Elperin T. New area rules for penetrating impactors. Int J Impact Eng 1998;21(1–2):51–9.
[14] Ben-Dor G, Dubinsky A, Elperin T. On the ballistic resistance of multi-layered targets with air gaps. Int J Solids Struct 1998;35:3097–103.
[15] Ben-Dor G, Dubinsky A, Elperin T. Analytical solution for penetration by rigid conical impactors using cavity expansion model. Mech Res Commun 2000;27:185–9.
[16] Ben-Dor G, Dubinsky A, Elperin T. Shape optimization of penetrator nose. Theor Appl Fract Mech 2001;35:261–70.